INPUT-OUTPUT CHARACTERIZATION OF AN ULTRASONIC TESTING SYSTEM BY DIGITAL SIGNAL ANALYSIS

James H. Williams, Jr., Samson S. Lee, and Hira Karagulle
Massachusetts Institute of Technology
Cambridge, Massachusetts 02139

The input-output characteristics of an ultrasonic testing system used for "stress wave factor" measurements were studied by coupling the transmitting and receiving transducers face to face, without a specimen in between. Some of the fundamentals of digital signal processing used are summarized.

The inputs and outputs were digitized and processed in a microcomputer by using digital signal-processing techniques. The entire ultrasonic test system, including transducers and all electronic components, was modeled as a discrete-time, linear, shift-invariant system. A digital bandpass filter was introduced to reduce noise effects on the output signal. The output due to a broadband input was deconvolved with the input to obtain the unit-sample response and the frequency response of the discrete-time system. Then the impulse response and frequency response of the continuous-time ultrasonic test system were estimated by interpolating the defining points in the unit-sample response and frequency response of the discrete-time system. The ultrasonic test system was found to behave as a linear-phase bandpass filter.

The unit-sample response and frequency response of the discrete-time model of the test system were used to compute the output of the test system for a variety of inputs. The agreement between predicted and measured outputs was excellent for rectangular pulse inputs of various amplitudes and durations and for tone burst and single-cycle inputs with center frequencies within the pass-band of the test system. The input-output limits on the linearity of the system were determined.

INTRODUCTION

Conventional ultrasonic testing (UT) is conducted either in the through-thickness transmission or pulse-echo modes (ref. 1). In the through-thickness transmission mode, the transmitting and receiving transducers are coupled to opposite faces of the structure under inspection, and the transmitted wave field is analyzed. In the pulse-echo mode, the transmitting and receiving transducers, which may be combined into a single transducer, are coupled to the same face of the structure under inspection, and the reflected wave field is analyzed.

Recently Vary et al. (refs. 2 and 3) introduced an ultrasonic nondestructive evaluation (NDE) parameter called the stress wave factor (SWF). It is similar to the pulse-echo test mode in that separate transmitting and receiving transducers are coupled to the same face of the structure. However, unlike conventional pulse-echo testing, which is generally limited to the analysis of nonoverlapping reflected wave echoes, the SWF is also valid for the analysis

of overlapping echoes. Specifically, an input pulse having a broadband frequency spectrum is applied to the transmitting transducer and the number of oscillations of the output signal at the receiving transducer exceeding a preselected voltage threshold is defined as the SWF. The SWF has been correlated with mechanical properties of carbon-fiber-reinforced composites (refs. 2 to 4). Williams et al. (ref. 5) theoretically and experimentally studied the ultrasonic input-output characteristics of the SWF test configuration in a thick, isotropic, elastic plate. The extension of that work to thin plates is currently in progress (ref. 6).

An important step toward the quantitative analysis of input-output relations in any ultrasonic NDE procedure is the quantitative characterization of the experimental test system without a test specimen. The effects on the output signal of the ultrasonic transducers, the coupling of the transducers to the test specimen, and electronic components such as filters, amplifiers, attenuators, and cables in the experimental system must be characterized before the test specimen's effects on the output signal can be isolated.

This study is part of an overall effort to develop quantitative analyses of the SWF and computer-aided nondestructive evaluation (CANDE, pronounced "candy") capabilities. The experimental UT system is characterized by directly coupling the transmitting and receiving transducers face to face without a test specimen. Input and output signals are digitized with a digital oscilloscope and are processed with a microcomputer by using digital signal-processing techniques. The transfer function of the experimental UT system without any test specimen was obtained.

The results of this study should provide a useful example in the characterization of any UT system that has separate transmitting and receiving transducers. Furthermore, developments in CANDE should be facilitated by the digital signal-processing procedures summarized herein.

FUNDAMENTALS OF DIGITAL SIGNAL PROCESSING

A few results in digital signal processing are summarized in this section. Digital signal-processing techniques are discussed extensively in the literature (refs. 7 to 10). Primarily, the notations in reference 7 are followed in this outline.

Digital signal processing is concerned with the representation of signals by sequences of numbers and the processing of those sequences. Sequences correspond to discrete-time signals derived from sampling continuous-time signals. The notation $x(n)$ denotes a sequence of numbers whose entries depend on the independent parameter n. The sequence $x(n)$ is defined only for integer values of n and represents successive samples of a continuous-time signal. For example, the sequence $x(n)$ is derived from periodic sampling of the continuous-time analog signal $x_a(t)$, where t is time, according to

$$x(n) = x_a(nT) \tag{1}$$

where T is the sampling period. The reciprocal of T is the sampling rate or sampling frequency. The availability of high-speed digital computers and efficient signal-processing algorithms has accelerated the implementation of

digital signal-processing techniques over that of continuous-time, analog signal-processing techniques. With the proper analysis, results from the digital signal processing of a sequence derived from sampling a continuous-time signal can accurately approximate results from continuous-time signal analyses.

A discrete-time system is defined mathematically as a unique transformation that maps an input sequence $x(n)$ into an output sequence $y(n)$. Discrete-time, linear, shift-invariant systems are discrete-time analogs of continuous-time, linear, time-invariant systems. Table 1 summarizes the input-output properties of discrete-time, linear and linear shift-invariant systems and their corresponding analogs in continuous-time systems. Discrete-time systems can be further characterized as stable and causal. A stable system is one for which every bounded input $x(n)$ produces a bounded output $y(n)$. A causal system is one for which the output $y(n)$ for n equal to n_0 depends only on the input $x(n)$ for n less than or equal to n_0. All subsequent discussions here are limited to discrete-time, linear, shift-invariant systems that are stable and causal.

The response of a linear, shift-invariant system can be characterized by the unit-sample response $h(n)$ via the convolution sum given in equation (1-1) in table 1. As a consequence, it can also be shown that the steady-state response of a linear, shift-invariant system to a sinusoidal input is sinusoidal of the same frequency as the input but with a magnitude and phase determined by the system. It is this property of linear, shift-invariant systems that makes representations of signals in terms of sinusoids or complex exponentials (i.e., Fourier representations) so useful in linear system theory. Also, it should be mentioned that the process of obtaining $y(n)$ from known $x(n)$ and $h(n)$ is called convolution, and the process of obtaining $h(n)$ from known $x(n)$ and $y(n)$ is called deconvolution.

Table 2 summarizes Fourier representations of continuous-time signals and of sequences. Fourier representations appear as equation pairs whose constituents are often referred to as the synthesis and analysis equations, as indicated in table 2. In equation (2-1b), $X_a(j\Omega)$ is a continuous function in radian frequency Ω and is the Fourier transform of the continuous-time signal $x_a(t)$, where the symbol j is defined as the square root of -1. If $x_a(t)$ has units of voltage, $X_a(j\Omega)$ has units of voltage per radian frequency (or simply volt-second); $X_a(j\Omega)$ is in general complex and can be specified by its magnitude and phase.

If $x_a(t)$ is a real-valued function of time, the magnitude and phase of $X_a(j\Omega)$ will be an even and odd function of frequency, respectively. Thus, it is only necessary to present the magnitude and phase of $X_a(j\Omega)$ for positive frequencies. If $x_a(t)$ is real and an even function of time, the phase of $X_a(j\Omega)$ is zero. If $x_a(t)$ is real and an odd function of time, the phase of $X_a(j\Omega)$ is $\pm\pi/2$. If $x_a(t)$ is shifted (i.e., advanced or delayed) in time, the magnitude of $X_a(j\Omega)$ is not affected, but a phase linearly proportional to frequency (i.e., linear phase) is introduced in the phase of $X_a(j\Omega)$. More specifically, the phase (in radians) is proportional to the radian frequency with a proportionality constant having units of time. The negative of the value of the proportionality constant is the time delay (ref. 9).

The remainder of table 2 deals with the Fourier representations of sequences. If properly computed, the Fourier transform $X_a(j\Omega)$ can be approximated by the Fourier representation of a sequence derived from sampling $x_a(t)$. Examples of the Fourier representations of continuous-time signals and sequences are illustrated in figure 1 and will be discussed shortly.

In equation (2-2b) in table 2 $X(e^{j\omega})$ is a continuous function of radian frequency ω and is the (discrete time) Fourier transform of a sequence $x(n)$. The frequency ω is in units of radians per increment of n, which is simply radians. If $x(n)$ has units of voltage, $X(e^{j\omega})$ has units of voltage per radian. The Fourier transform of a sequence is useful for analyzing general sequences. The discrete Fourier series representations of a periodic sequence $x(n)$ of period N are also shown in table 2. A periodic sequence $\tilde{x}(n)$ of period N is one such that $\tilde{x}(n)$ equals $\tilde{x}(n + N)$. In equation (2-3b) $\tilde{X}(k)$ is a periodic sequence of period N, and the numbers in this sequence are the discrete Fourier series coefficients of the periodic sequence $\tilde{x}(n)$ having period N. If $\tilde{x}(n)$ has units of voltage, $\tilde{X}(k)$ has units of voltage also. The discrete Fourier series of a periodic sequence serves as a prelude to the discrete Fourier transform (DFT). In equation (2-4b) $X(k)$ is a sequence of length N and is called the DFT of a finite-length sequence $x(n)$ of length N (ref. 7). If $x(n)$ has units of voltage, $X(k)$ has units of voltage also. The DFT is useful for digital signal processing because sequences processed by a computer are of finite length and also because efficient DFT computational algorithms are available.

By comparing the entries in table 2 for the discrete Fourier series of a periodic sequence of period N and the DFT of a finite-length sequence of length N, it is observed that the DFT representation is obtained from the discrete Fourier series representation by interpreting the finite-length sequence as one period of a periodic sequence. The properties of the DFT are similar to those of the Fourier transform, except that because of the implied periodicity, shifts of $x(n)$ in n by one period N and an integer multiple of one period are indistinguishable and a shift in n of larger than N is the same as a shorter shift.

The DFT was computed via a fast Fourier transform (FFT) algorithm. The inverse DFT computed via an inverse FFT (IFFT) algorithm was used to evaluate $x(n)$ from $X(k)$. The FFT computation is particularly efficient when the length of the sequence is an integer power of 2. A sequence of length N is called an N-point sequence. The DFT of an N-point sequence is called an N-point DFT and is computed via an N-point FFT algorithm. Figure 1 illustrates that the Fourier transform of a continuous-time signal can be reconstructed approximately from the DFT of a sequence derived from sampling the continuous-time signal. Again, note that where DFT relations are concerned, a finite-length sequence is represented as one period of a periodic sequence.

Figure 1 shows Fourier representations of continuous-time signals and of sequences derived from sampling the continuous-time signals. In part (i) of figure 1(a), the continuous-time signal $x_a(t)$ is assumed to be bandlimited in frequency with Fourier representation $X_a(j\Omega)$ as shown. The highest frequency of $x_a(t)$ is assumed to be $\Omega_0/2$. In part (ii) of figure 1(a), a sequence $x(n)$ results from the periodic sampling of $x_a(t)$ with a sampling ing period of T. The Fourier transform of the sequence $x(n)$ into a continuous function $X(e^{j\omega})$ is also shown. It is observed that $X(e^{j\omega})$ can be obtained from $X_a(j\Omega)$ by the superposition of an infinite number of $X_a(j\Omega)$

shifted in frequency ω by integer multiples of 2π. The magnitude and frequency of $X(e^{j\omega})$ are scaled from those of $X_a(j\Omega)$ by $1/T$ and T, respectively. The Fourier transform $X_a(j\Omega)$ can be recovered exactly, except for the scaling factors, from the Fourier transform $X(e^{j\omega})$ of the sequence $x(n)$ in the interval of $-\pi \leq \omega \leq \pi$ by low-pass filtering $X(e^{j\omega})$ with a cutoff frequency of π, on one condition. The condition is that $\Omega_0 T/2 < \pi$ so that there will be no overlapping of superposed $X_a(j\Omega)$ in forming $X(e^{j\omega})$. This condition is known as the "sampling theorem" and assures that if a continuous-time signal $x_a(t)$ is sampled at a frequency greater than twice the highest frequency of $x_a(j\Omega)$, then $X(e^{j\omega})$ is identical to $X_a(j\Omega)$ in the interval $-\pi \leq \omega \leq \pi$, except for scaling factors. Because $X_a(j\Omega)$ is recovered, the continuous-time signal $x_a(t)$ can be recovered from the sequence $x(n)$. This minimum required sampling frequency is called the Nyquist rate or the Nyquist frequency (refs. 7, 9, and 10). The distortion due to overlapping of superposed $X_a(j\Omega)$ when the sampling theorem is violated is called aliasing. In part (ii) in figure 1(a), the case where there is no overlapping of superposed $X_a(j\Omega)$ is illustrated; thus the signal is not aliased.

Whereas figure 1(a) deals with general continuous-time signals, figure 1(b) deals with finite-duration continuous-time signals. In part (i) in figure 1(b), a continuous-time signal $x_a(t)$ with nonzero values over a finite time duration and its Fourier representation $X_a(j\Omega)$ are shown. The duration where the signal is nonzero is assumed to be t_0, and sampling the continuous-time signal with a sampling period T is assumed to result in a sequence of length N. It is observed that $X_a(j\Omega)$ for a finite-duration signal is not bandlimited in frequency. In part (ii) in figure 1(b), a sequence $x(n)$ results from the periodic sampling of $x_a(t)$ with a sampling period of T. All numbers in the sequence $x(n)$ are zero for $n < 0$ and for $n > N - 1$. Thus $x(n)$ is a finite-length sequence of length N. The Fourier transform of the sequence $x(n)$ into the continuous function $X(e^{j\omega})$ is also shown. Similar to the results in figure 1(a), $X(e^{j\omega})$ can be obtained from $X_a(j\Omega)$ by the superposition of an infinite number of $X_a(j\Omega)$ shifted in frequency ω by integer multiples of 2π. However, for this case, because $X_a(j\Omega)$ is not bandlimited in frequency, there is overlapping of superposed $X_a(j\Omega)$ in forming $X(e^{j\omega})$. Thus there is aliasing and $X_a(j\Omega)$ cannot be recovered exactly from $X(e^{j\omega})$ in the interval $-\pi \leq \omega \leq \pi$. However, if the sampling frequency is greater than twice most of the significant frequency components in $X_a(j\Omega)$, then $X_a(j\Omega)$ can still be approximated adequately by $X(e^{j\omega})$. The DFT $X(k)$ of the finite-length sequence $x(n)$ is often computed instead of $X(e^{j\omega})$. However, in DFT evaluations, a finite-length sequence is represented as one period of a periodic sequence.

In part (iii) of figure 1(b), a periodic sequence $\tilde{x}(n)$ of period N constructed by using the N-point sequence $\tilde{x}(n)$ as a period is shown. The discrete Fourier series representation $\tilde{X}(k)$ of the periodic sequence $\tilde{x}(n)$ is also shown; $\tilde{X}(k)$ is a periodic sequence of period N. The DFT $X(k)$ of the finite-length sequence $x(n)$ can be interpreted as a period of $\tilde{X}(k)$ for $0 \leq k \leq N - 1$ as shown. It is observed that $X(e^{j\omega})$ can be obtained from $\tilde{X}(k)$ by interpolating points in $\tilde{X}(k)$. Because $X_a(j\Omega)$ can be approximated adequately by $X(e^{j\omega})$ if the sampling frequency is greater than twice most of the significant frequency components in $X_a(j\Omega)$, interpolations of $\tilde{X}(k)$ or $X(k)$ can be used to estimate $X_a(j\Omega)$. The numbers in $X(k)$ are scaled approximately from the values of $X_a(j\Omega)$ by a factor of $1/T$, and the spacing between successive numbers in the sequence $X(k)$ can be interpreted as $2\pi/(NT)$

in radian frequency, which is the frequency domain resolution. Again, the reconstruction of the Fourier transform of a finite-duration, continuous-time signal from the DFT of a finite-length sequence by interpolation is generally an approximation due to aliasing.

Table 3 lists the conditions for the special case where there is exact correspondence (to within a scaling factor) of the Fourier transform of a continuous-time signal and the DFT of a finite-length sequence derived from sampling (ref. 10). Also, the N-point sequence $x(n)$ can be considered as an M-point sequence if M is greater than N with the last $M-N$ numbers in the M-point sequence being zero. As discussed here next regarding convolution procedures, sometimes it is convenient to extend the length of a sequence by appending zeroes.

Because the response of a linear, shift-invariant system can be evaluated via the convolution sum in equation (1-1) in table 1, convolution representations are discussed here. Table 4 summarizes convolution representations of continuous-time signals and of sequences. The Fourier representations of the convolutions are also given in table 4. Equation (4-1a) gives the linear convolution of continuous-time signals $x_{a1}(t)$ and $x_{a2}(t)$, resulting in $x_{a3}(t)$. The Fourier representation of the convolution is given in equation (4-1b). Convolution in the time domain results in multiplication in the frequency domain. Conversely, because of the duality between time and frequency domains in Fourier representations, convolution in the frequency domain results in multiplication in the time domain, such as time windowing (ref. 9). The concepts of periodic and circular convolutions are introduced as preludes to the efficient evaluation of linear convolution of sequences using DFT procedures.

Equation (4-2a) in table 4 gives the periodic convolution of two periodic sequences $\tilde{x}_1(n)$ and $\tilde{x}_2(n)$, each of period N, resulting in a periodic sequence $\tilde{x}_3(n)$ of period N. By restricting attention to one period of the periodic convolution, circular convolution of two N-point sequences $x_1(n)$ and $x_2(n)$ to obtain an N-point sequence $x_3(n)$ can be defined from the periodic convolution and is given in equation (4-3a). The two periodic sequences $\tilde{x}_1(n)$ and $\tilde{x}_2(n)$, each of period N, are constructed by using the N-point sequences $x_1(n)$ and $x_2(n)$ as periods, respectively. Equations (2-3b) and (2-4b) in table 2 have been used to obtain the simplified equation (4-3b) because $\tilde{x}_1(n)$ and $\tilde{x}_2(n)$ are equal to $x_1(n)$ and $x_2(n)$ for n ranging from zero to $N - 1$. Thus $\tilde{X}_1(k)$ and $\tilde{X}_2(k)$ for $0 \leq k \leq N - 1$ become $X_1(k)$ and $X_2(k)$, respectively. The circular convolution of N-point sequences is called an N-point circular convolution. The designation "circular" is derived from a graphical representation of how an N-point sequence can be used to construct a periodic sequence of period N (ref. 7). It can be imagined that the N points from the N-point sequence are equally spaced in angle around a circle with a circumference of exactly N points. The periodic sequence of period N is obtained by traveling around the circumference of the circle a number at a time recording the N-point sequence repeatedly. Also, a rotation of the circle corresponds to circular shifting of the N-point sequence (ref. 7).

The linear convolution of an N_1-point sequence $x_1(n)$ and an N_2-point sequence $x_2(n)$ is defined as

$$x_3(n) = \sum_{m=0}^{N_1-1} x_1(m)\, x_2(n - m) \tag{2}$$

Because the resulting sequence $x_3(n)$ is of length $N_1 + N_2 - 1$ (ref. 7), the evaluation of linear convolution via circular convolution requires all sequences to be of the same length, which has to be $N_1 + N_2 - 1$. Equation (4-4a) in table 4 gives the linear convolution of finite-length sequences $x_1(n)$ and $x_2(n)$ to obtain a finite-length sequence $x_3(n)$ evaluated via circular convolution. Computation of circular convolution using DFT is preferred over the direct evaluation of linear convolution because of computational efficiencies. The $(N_1 + N_2 - 1)$-point DFT's of the two convolving sequences are computed via an FFT algorithm and then multiplied according to equation (4-4b). The $(N_1 + N_2 - 1)$-point inverse DFT of the product is computed via an IFFT algorithm, and the result is the desired linear convolution. Because the original sequences $x_1(n)$ and $x_2(n)$ are of lengths N_1 and N_2, respectively, $N_2 - 1$ and $N_1 - 1$ zeroes are appended to $x_1(n)$ and $x_2(n)$, respectively, to yield two $(N_1 + N_2 - 1)$-point sequences for the $(N_1 + N_2 - 1)$-point circular convolution. Alternatively, if linear convolution of two $(N_1 + N_2 - 1)$-point sequences is conducted via an $(N_1 + N_2 - 1)$-point circular convolution, the last $N_2 - 1$ numbers in one sequence to be convolved must be zeroes and the last $N_1 - 1$ numbers in the other sequence to be convolved must be zeroes. In practice, the sequences are extended to a length that is greater than $N_1 + N_2 - 1$ and is an integer power of 2 for efficient FFT computation.

Figure 2 shows convolution representation of continuous-time signals and their sequences derived by sampling. In figure 2(a), continuous-time signals $x_{a1}(t)$ of duration t_1 and $x_{a2}(t)$ of duration t_2 are convolved to form the continuous-time signal $x_{a3}(t)$ of duration $t_1 + t_2$. In part (i) of figure 2(b), the continuous-time signal $x_{a1}(t)$ is sampled with a sampling period T and is assumed to produce an N_1-point sequence. Then $N_2 - 1$ zeroes are appended to form an $(N_1 + N_2 - 1)$-point sequence $x_1(n)$. Next a periodic sequence $\tilde{x}_1(n)$ of period $N_1 + N_2 - 1$ is constructed by using $x_1(n)$ as a period. Similarly, in part (ii) in figure 2(b), the periodic sequence $\tilde{x}_2(n)$ of period $N_1 + N_2 - 1$ is obtained from $x_{a2}(t)$, which is assumed to produce an N_2-point sequence when sampled with a sampling period T. Periodic convolution of $\tilde{x}_1(n)$ and $\tilde{x}_2(n)$ results in the periodic sequence $\tilde{x}_3(n)$. Then $x_3(n)$ can be identified from the circular convolution portion of $\tilde{x}_3(n)$ by restricting attention to one period of the periodic sequence. It is observed that $x_{a3}(t)$ can be approximated from the interpolation of the $(N_1 + N_2 - 1)$-point sequence $x_3(n)$. The numbers in $x_3(n)$ are scaled approximately from the value of $x_{a3}(t)$ by a factor of $1/T$ and the spacing between successive numbers in the sequence $x_3(n)$ can be interpreted as T. Because the circular convolution is obtained via a DFT, restrictions on the DFT apply to the convolution also. Thus the sampling theorem applies to sampling the continuous-time signals if $x_{a3}(t)$ is to be approximated adequately by the sequence $x_3(n)$.

In practice, if a continuous-time signal is to be sampled, the sampling frequency and the sampling length must be specified. Table 5 summarizes the significance of the sampling parameters. Equation (5-1) is based on the earlier discussion in relation to figure 1(a).

EXPERIMENTAL SYSTEM

A schematic of the experimental system including the specimen is shown in figure 3. This is a typical stress-wave-factor test configuration. The goal

of this study was to characterize the experimental test system without the test specimen. Thus, all testing in this study was conducted with the transmitting and receiving transducers directly coupled face to face without any test specimen in between.

The system consisted of a pulse/function generator (Wavetek model 191); a 5-MHz (corresponding to -3-dB point) low-pass filter (Allen Avionics F2516); broadband (0.1 to 3.0 MHz) transmitting and receiving transducers (Parametrics V105) having an approximately flat sensitivity of -85 dB relative to 1 V/μbar; an ultrasonic interface couplant (Acoustic Emission Technology SC-6); an ultrasonic preamplifier (custom built by Parametrics) having a gain of 40 dB in the frequency bandwidth 1 kHz to 10 MHz; a variable-frequency filter (A.P. Circuit Corporation AP 220-5), which could be used as a low-pass, high-pass, bandpass, or bandstop filter in the frequency range 10 Hz to 2.5 MHz; a digital oscilloscope (Nicolet model 2090 with plug-in model 204-A), which could sample and store analog signals at sampling frequencies from 0.05 Hz to 20 MHz (corresponding to sampling periods from 20 sec to 50 nsec) up to 4096 points; and an IBM personal computer (IBM PC), which was interfaced with the digital oscilloscope.

The variable-frequency filter was used as a 0.4- to 2.6-MHz (corresponding to -3-dB points) bandpass filter, selected on the basis of the receiving transducer frequency response. All signals were sampled at a sampling frequency of 20 MHz (i.e., one sample every 50 nsec) for 256 points. Thus each recorded signal was 12.8 μsec in duration. The 5-MHz low-pass filter was selected via antialiasing considerations. Table 6 is a BASIC language program listing for the FFT and IFFT computations used in this study. All DFT and inverse DFT evaluations in this study were conducted by using this program.

DIGITAL CHARACTERIZATION OF EXPERIMENTAL SYSTEM

The objective of this study was to obtain the system transfer characteristics between the input to the transmitting transducer and the output from the receiving transducer after signal conditioning. A schematic of the experimental system is shown in figure 3. Once again, note that the experiment was conducted with the transmitting and receiving transducers coupled face to face without a test specimen. Thus, the "system" under study consisted of the transmitting transducer, the coupling between transmitting and receiving transducers, the receiving transducer, the ultrasonic preamplifier, the variable-frequency filter, and all necessary cables.

A continuous-time system can be described by its impulse response $h_a(t)$ and its frequency response $H_a(j\Omega)$. In this study, the $h_a(t)$ and $H_a(j\Omega)$ of the test system were computed from the unit-sample response $h(n)$ and the DFT of $h(n)$ denoted $H(k)$, respectively, of a discrete-time model of the continuous-time system.

The experimental system was assumed to be a discrete-time, linear, shift-invariant system. As shown in figure 3, channel 1 of the digital oscilloscope sampled the continuous-time input signal to the transmitting transducer. The resulting discrete-time signal is called the input sequence and is denoted by $x(n)$. Similarly, channel 2 of the digital oscilloscope sampled the continuous-time output signal from the receiving transducer after preamplification and bandpass filtering. The resulting discrete-time signal is called the output

sequence and is denoted by $y(n)$. Thus, the objective of this study was to obtain the discrete-time system transfer characteristics between $x(n)$ and $y(n)$. The discrete-time system besides being linear and shift-invariant was observed to be stable and causal. A schematic of the digital signal-processing procedures applied to obtain the unit-sample response and frequency response of the discrete-time system is shown in figure 4.

The pulse/function generator produced an approximately rectangular pulse 20 nsec in duration. The rectangular pulse was passed through the 5-MHz low-pass filter before it reached the digital oscilloscope. Figure 5 shows the time histories of the input and output signals by linearly interpolating the defining points in the input and output sequences $x(n)$ and $y(n)$. The input and output signals were approximately 3 and 4 μsec long, respectively. Thus for the sampling period 50 nsec, only approximately the first 60 and 80 numbers in the sequences $x(n)$ and $y(n)$, respectively, were nonzero. Actually, the sequences $x(n)$ and $y(n)$ were of length 256 after sampling; that is, the digital oscilloscope recorded 256 points each for the input and output signals. Then 768 zeroes were appended to the sequences to produce $x(n)$ and $y(n)$ of length 1024. Extended sequences were used to facilitate evaluation of linear convolution via the DFT, as discussed later. The DFT's $X(k)$ and $Y(k)$ for $x(n)$ and $y(n)$, respectively, were evaluated by using a 1024-point FFT algorithm based on 1024-point $x(n)$ and $y(n)$. Because the input and output signals were of finite duration, they were not bandlimited in frequency. However, because the sampling frequency (20 MHz) was greater than most of the significant frequency components in the input signal (significant up to 5 MHz) and the output signal (significant up to 2.6 MHz), the sampling theorem assured an adequate approximation of the Fourier transform of the input and output signals by the DFT of the input and output sequences. Approximations of the magnitude and phase of the Fourier transform of the input and output signals are shown in figure 5. The magnitude and phase of the Fourier transform were obtained by linearly interpolating the defining points in the magnitude and phase of the DFT of the input and output sequences. The magnitude shown in figure 5 is presented on a decibel scale, normalized with respect to the magnitude of the largest component in the Fourier transform. The magnitudes of the largest components in the Fourier transforms of the input and output were 2.3×10^{-7} and 9.3×10^{-7} V-sec, corresponding to frequencies of 0.4 and 1.4 MHz, respectively. When the magnitude was small, both the magnitude and the phase were erratic because of sensitivity to noise contamination (fig. 5).

Letting the 1024-point DFT of the unit-sample response $h(n)$ of the discrete-time system be defined as $H(k)$, we can then use equation (4-4b) in table 4 to relate the DFT of the input $X(k)$ and the DFT of the output $Y(k)$ as

$$Y(k) = H(k)\, X(k) \tag{3}$$

where $0 \leq k \leq 1023$ for this case. Then $H(k)$ for the system can be evaluated by rearranging equation (3) as

$$H(k) = Y(k)/X(k) \tag{4}$$

The inverse DFT of $H(k)$ is the desired unit-sample response $h(n)$. The procedure for obtaining $h(n)$ from known $x(n)$ and $y(n)$ is called deconvolution.

However, results from attempts to perform the direct division in equation (4), using $X(k)$ and $Y(k)$, as shown in figure 5, were unsatisfactory because of noise. Thus, the output $y(n)$ was filtered digitally before division. The digital filter was selected by trial and error. Various digital filters were applied, and the resulting $H(k)$ and the unit-sample response $h(n)$ were used to evaluate output properties for various inputs and were compared with experimental results. The digital filter selected was a bandpass filter utilizing time windowing via a 701-point Blackman window (ref. 7). Specifically, the digital filter was obtained via the following steps: (1) obtain the unit-sample response $h_d(n)$ of a desired ideal bandpass filter of 0.2 to 4.5 MHz, (2) shift $h_d(n)$ by 350 points to obtain the unit-sample response $h_3(n)$, and (3) multiply $h_3(n)$ by a 701-point Blackman window $w_1(n)$ to obtain a 701-point unit-sample response $h_4(n)$ of the filter. These steps are illustrated in figure 4 also. The resulting digital filter was a causal, linear-phase bandpass filter. Step 1 identified the desired bandpass filter. Because an ideal filter is noncausal, as indicated by its $h_d(n)$, which is nonzero for n less than zero, step 2 shifted $h_d(n)$ by delaying it by 350 points. A causal filter is especially important for real-time signal processing.

Because the desired digital filter was a finite impulse response (FIR) filter, which by definition should have a unit-sample response of finite duration (ref. 7), $h_3(n)$ was truncated and only numbers between n of zero and 701, inclusively, were retained. To minimize the effects of truncation, $h_3(n)$ was multiplied by a 701-point Blackman window $w_1(n)$ in step 3 to form $h_4(n)$. The length of 701 points minimized the effects of truncation and yet allowed a 1024-point DFT evaluation. The length of the sequence $h_4(n)$ of the filter affected the DFT evaluation because filtering in the frequency domain (i.e., multiplying the responses of the filter and the signal in the frequency domain) corresponded to convolution in the time domain. Because only the first 80 numbers in the sequence $y(n)$ were nonzero, proper evaluation of the linear convolution of the sequence $y(n)$ with the sequence $h_4(n)$, which was nonzero for the first 701 numbers, required at least a 780-point DFT, according to discussions associated with equation (4-4) in table 4. By increasing the number of points to the nearest integer power of 2, which for this case was 1024, 1024-point sequences and 1024 DFT's resulted. Thus, sufficient zeroes were appended to any sequence to extend its length to 1024 points, unless otherwise indicated. Also, 1024-point DFT's evaluated via a 1024-point FFT were used, unless otherwise indicated.

The 1024-point DFT of the unit-sample response of the digital bandpass filter designed by time windowing the unit-sample response of an ideal bandpass filter with a Blackman window is denoted by $H_2(k)$. Using equation (4-4b) in table 4, the DFT of the output after digital filtering was $H_2(k)\ Y(k)$. Then equation (4) could be modified as

$$H_1(k) = H_2(k)\ Y(k)/X(k) \tag{5}$$

where $H_1(k)$ was an approximation to $H(k)$, and $0 \leq k \leq 1023$.

The unit-sample response $h_1(n)$ was obtained from $H_1(k)$ by performing an inverse DFT via an IFFT algorithm. Because $h_1(n)$ corresponded to $h_a(t)$, which is a real function of time, $h_1(n)$ was a sequence of real numbers and corresponded to the real part of the IFFT. Because a shift of 350 points (corresponding to 17.5 μsec) was introduced in the design of the causal, digital

bandpass filter, the unit-sample response $h_1(n)$ had to be shifted back by 350 points to remove the artifact introduced by the digital filter. This was done after the rectangular windowing procedure discussed in the next paragraph.

The individual values in the sequence $h_1(n)$ for $n \leq 355$ and $n \geq 450$ were small, less than $1/100^{th}$ of the maximum value in the sequence. These small values were due to noise contamination introduced during signal recording and also by the digital filtering. So, the sequence $h_1(n)$ was time windowed by a rectangular window $w_2(n)$ defined by

$$w_2(n) = \begin{cases} 1 \text{ for } 355 < n < 450 \\ 0 \text{ otherwise} \end{cases} \tag{6}$$

Thus, the numbers in $h_1(n)$ were not affected for $355 < n < 450$, but all others had been set to zero. The resulting sequence obtained by multiplying $h_1(n)$ and $w_2(n)$ is denoted as $h_2(n)$. This time windowing significantly smoothed the phase of $H_1(k)$ in the high-frequency region.

After the rectangular windowing, the sequence $h_2(n)$ was shifted back 350 points to remove the shift (i.e., time delay) introduced by the bandpass digital filter discussed earlier. The 1024-point sequence $h_2(n)$ was shifted to obtain $h(n)$ according to circular shifting, which in this case became

$$h(n) = \begin{cases} h_2(n + 350) & \text{for } 0 \leq n \leq 1023 - 350 \\ h_2(n - 1024 + 350) & \text{for } 1024 - 350 \leq n \leq 1023 \\ 0 & \text{otherwise} \end{cases} \tag{7}$$

The sequence $h(n)$ was the unit-sample response of the test system. The numbers in $h(n)$ were zero for $n \geq 100$ due to the windowing described in equation (6). Circular shifting was used instead of linear shifting because $h_2(n)$ was the result of a few DFT evaluations and, when a DFT evaluation was performed, a finite-length sequence was implied as a period of a periodic sequence. Thus, circular shifting procedures corresponding to shifting a periodic sequence were required.

The DFT of the unit-sample response $h(n)$ was $H(k)$. Because $h(n)$ was nonzero only for <100, the first 512 points of $h(n)$ were used to compute $H(k)$ via a 512-point FFT. Thus, $H(k)$ as obtained was a 512-point sequence; $H(k)$ was the frequency response of the discrete-time model of the test system.

Figure 6(a) shows the impulse response $h_a(t)$ of the test system as obtained by linearly interpolating the defining points in the unit-sample response $h(n)$. An impulse response has units of response per unit of excitation multiplied by time (ref. 11). Thus, $h_a(t)$ in figure 6(a) is shown with units of volts per volt-second. The duration of the unit-sample response was approximately 3 μsec. Figure 6(b) shows the magnitude and phase of the frequency response $H_a(j\Omega)$ of the test system as estimated by linearly interpolating the defining points in the frequency response $H(k)$. A frequency response magnitude has units of response per unit of excitation (ref. 11). Thus, the magnitude of $H_a(j\Omega)$ has units of volts per volt. The magnitude of $H_a(j\Omega)$ is shown in figure 6(c) on a decibel scale, normalized with respect to the magnitude of the largest component in $H_a(j\Omega)$, which is

2.7×10^{-7} V/V corresponding to a frequency of 1.7 MHz. The normalized magnitude had a maximum value at 1.7 MHz, and the values of the normalized magnitude decreased by 6 dB from the maximum value at 0.6 and 2.3 MHz. The phase of $H_a(j\Omega)$ was linear from 0.3 to 2.7 MHz. The linear-phase behavior indicates that inputs of frequencies from 0.3 to 2.7 MHz will result in outputs delayed in time without distortion. (However, distortion occurred because the magnitude of $H_a(j\Omega)$ was not constant from 0.3 to 2.7 MHz.) The introduced time delay corresponding to the linear phase can be computed to be 0.49 μsec. As shown by the magnitude plot, the system was insensitive to frequencies below 0.6 MHz and above 2.3 MHz; the information in these frequencies was easily contaminated by noise and also displayed the effects of digital filtering. Thus, to summarize, the system behaved as a linear-phase bandpass filter in the frequency range 0.6 to 2.3 MHz.

RESULTS AND DISCUSSION

The outputs of the test system due to different inputs can be predicted by using the unit-sample response $h(n)$ and frequency response $H(k)$ of the discrete-time model of the test system. If the input is $x(n)$ and the output is $y(n)$, the input-output relationship is given by the convolution in equation (1-1) in table 1. For finite-length sequences, equation (1-1) can be written in a similar form as equation (2). The convolution is conveniently evaluated via the DFT. If the DFT of the input is $X(k)$, the DFT of the output $Y(k)$ can be evaluated by using equation (3). So, the output $y(n)$ due to the input $x(n)$ is the inverse DFT of $Y(k)$. The frequency response $H(k)$ is shown in figure 6. Figures 7 to 10 show the outputs of the system to various inputs. The time histories of the predicted outputs were obtained by linearly interpolating the defining points in the sequence $y(n)$ as obtained via the DFT procedure for 512-point DFT's.

Figures 7 and 8 show the outputs of the system to tone burst inputs of approximately 6 μsec in duration and 1.5 and 2.5 MHz in center frequency, respectively. The agreement between the experimentally measured and the predicted outputs was excellent. The arrival times of peaks of individual cycles were predicted to within ±25 nsec in both cases. The measured peak amplitudes of all the individual cycles were correctly predicted to within maximum errors of 5 and 9 percent for the 1.5- and 2.5-MHz inputs, respectively. Similar agreement was also obtained for center frequencies ranging from 0.5 to 3 MHz.

Figure 9 shows the output of the system to a 7.5-μsec-duration rectangular pulse input. The agreement between the experimentally measured and the predicted outputs was excellent. The arrival times of peaks of individual cycles were predicted to within ±25 nsec. The measured peak amplitudes of the individual cycles were correctly predicted to within a maximum error of 5 percent. From figure 9, for the approximate time of 5 to 7 μsec, both the measured and the predicted outputs were constant in time. The constant values corresponded to 0 and 0.046 V for the measured and predicted outputs, respectively. Similar agreement was also obtained for pulse durations ranging down to 0.85 μsec.

Figure 10 shows the output of the system to one cycle of 1.75-MHz-frequency input at 2.3 V peak to peak. The arrival times of peaks of individual cycles were predicted to within ±25 nsec. The shapes of the measured and predicted outputs agreed well, but the amplitude of the predicted output was somewhat larger than that of the measured output. As shown in figure 10, the predicted and measured peak-to-peak output amplitudes were 8.7 and 7.2 V, respectively. The predicted output was larger than the measured output when the input and output exceeded 1.4 and 5.1 V peak to peak, respectively. This nonlinearity indicates that the linear model used in the prediction becomes inadequate for large-amplitude inputs and outputs. When the input and output were less than 1.4 and 5.1 V peak to peak, respectively, the measured output peak amplitudes were correctly predicted to within a maximum error of 6 percent. Restrictions on both input and output amplitudes were imposed because the nonlinearity may be due to the input or the output or both.

CONCLUSIONS

The SWF ultrasonic test system input-output characteristics were investigated by directly coupling the transmitting and receiving transducers face to face without a test specimen. Some of the fundamentals of digital signal processing were summarized. Input and output signals were digitized by using a digital oscilloscope, and the digitized data were processed in a microcomputer by using digital signal-processing techniques.

The continuous-time test system was modeled as a discrete-time, linear, shift-invariant system. In estimating the unit-sample response and frequency response of the discrete-time system, it was necessary to use digital filtering to remove low-amplitude noise, which interfered with deconvolution calculations. A digital bandpass filter constructed with the assistance of a Blackman window and a rectangular time window were used. Approximations of the impulse response and the frequency response of the continuous-time test system were obtained by linearly interpolating the defining points of the unit-sample response and the frequency response of the discrete-time system. The test system behaved as a linear-phase bandpass filter in the frequency range 0.6 to 2.3 MHz. These frequencies were selected in accordance with the criterion that they were 6 dB below the maximum peak of the amplitude of the frequency response.

Furthermore, by using the unit-sample response and the frequency response of the discrete-time system and the assumption of a linear, shift-invariant system, the output of the system to various inputs was predicted and the results were compared with the corresponding measurements on the system. The predicted output was obtained by linearly interpolating the defining points of the discrete-time output sequence. Tone bursts of various center frequencies and durations, rectangular pulses of various durations, and angle cycle inputs at 1.75 MHz with various amplitudes were considered. Excellent agreement between the predicted and measured results was obtained for tone bursts with center frequencies from 0.5 to 3 MHz and rectangular pulses. Excellent agreement between the predicted and measured results was also obtained for one-cycle inputs of various amplitudes, as long as the input and output were less than 5.1 V peak to peak, respectively, at a 40-dB system gain. These results are specific for the particular set of components in the test system.

The results of this study will be useful in the quantitative analysis of the SWF when test specimens are inserted between the transducers. With known test system characteristics, the effects on the output signal due to the test specimen having a variety of flaw states can be isolated. Furthermore, using and discussing digital signal-processing methods extensively may facilitate developments in CANDE.

REFERENCES

1. J. Krautkramer and H. Krautkramer, Ultrasonic Testing of Materials, Second Edition, Springer-Verlag, N.Y., 1977.

2. A. Vary and R.F. Lark, "Correlation of Fiber Composite Tensile Strength with the Ultrasonic Stress Wave Factor", Journal of Testing and Evaluation, vol. 7, no. 4, July 1979, pp. 185-191.

3. A. Vary and K.J. Bowles, "An Ultrasonic-Acoustic Technique for Nondestructive Evaluation of Fiber Composite Quality", Polymer Engineering and Science, vol. 19, no. 5, Apr. 1979, pp. 373-376.

4. J.H. Williams, Jr., and N.R. Lampert, "Ultrasonic Evaluation of Impact-Damaged Graphite Fiber Composite", Materials Evaluation, vol 38, no. 12, Dec. 1980, pp. 68-72.

5. J.H. Williams, Jr., H. Karagülle, and S.S. Lee, "Ultrasonic Input-Output for Transmitting and Receiving Longitudinal Transducers Coupled to Same Face of Isotropic Elastic Plate", Materials Evaluation, vol. 40, no. 6, May 1982, pp. 655-662.

6. H. Karagülle, "Ultrasonic Input-Output for Transmitting and Receiving Transducers Coupled to Same Face of Isotropic Elastic Plates", Doctoral Thesis Proposal, Submitted to the Department of Mechanical Engineering, Massachusetts Institute of Technology, Cambridge, Mass., Oct. 1982.

7. A.V. Oppenheim and R.W. Schafer, Digital Signal Processing, Prentice-Hall, Inc., Englewood Cliffs, N.J., 1975.

8. S.D. Stearns, Digital Signal Analysis, Hayden Book Company, Inc., Rochelle Park, N.J., 1975.

9. A.V. Oppenheim, A.S. Willsky, with I.T. Young, Signals and Systems, Prentice-Hall, Inc., Englewood Cliffs, N.J., 1983.

10. E.O. Brigham, The Fast Fourier Transform, Prentice-Hall, Inc., Englewood Cliffs, N.J., 1974.

11. S.H. Crandall and W.D. Mark, Random Vibration in Mechanical Systems, Academic Press, N.Y., 1963.

TABLE 1 Input-Output Properties of Discrete-Time Linear, Shift-Invariant and Linear Shift-Invariant Systems and Their Corresponding Analogs in Continuous-Time Systems.

Discrete-Time System	System Input-Output Properties	Analog in Continuous-Time System
Linear	If $x_1(n) \rightarrow y_1(n)$ and $x_2(n) \rightarrow y_2(n)$, then $ax_1(n) + bx_2(n) \rightarrow ay_1(n) + by_2(n)$ (Principle of Superposition)	Linear
Shift-Invariant	If $x(n) \rightarrow y(n)$, then $x(n - k) \rightarrow y(n - k)$	Time-Invariant
Linear Shift-Invariant	If $\delta(n) \rightarrow h(n)$, then $x(n) \rightarrow y(n)$ where $y(n) = \sum_{k=-\infty}^{\infty} x(k)h(n - k)$ (1-1)* (Convolution Sum)	Linear Time-Invariant

* $\delta(n)$ is called the unit-sample sequence and is given by

$$\delta(n) = \begin{cases} 1, & n = 0 \\ 0, & n \neq 0 \end{cases} \qquad (1\text{-}2)$$

and $h(n)$ is called the unit-sample response.

TABLE 2 Fourier Representations of Continuous-Time Signals and of Sequences.

Fourier Representation	Synthesis Equation	Analysis Equation
Fourier transform of continuous-time signal $x_a(t)$	$x_a(t) = \frac{1}{2\pi}\int_{-\infty}^{\infty} X_a(j\Omega)e^{j\Omega t}d\Omega$ (2-1a)	$X_a(j\Omega) = \int_{-\infty}^{\infty} x_a(t)e^{-j\Omega t}dt$ (2-1b)
Fourier transform of sequence x(n) into the continuous function $X(e^{j\omega})$	$x(n) = \frac{1}{2\pi}\int_{-\pi}^{\pi} X(e^{j\omega})e^{j\omega n}d\omega$ (2-2a)	$X(e^{j\omega}) = \sum_{n=-\infty}^{\infty} x(n)e^{-j\omega n}$ (2-2b)
Discrete Fourier series of periodic sequence $\tilde{x}(n)$ of period N	$\tilde{x}(n) = \frac{1}{N}\sum_{k=0}^{N-1} \tilde{X}(k)e^{jk(2\pi/N)n}$ (2-3a)	$\tilde{X}(k) = \sum_{n=0}^{N-1} \tilde{x}(n)e^{-jk(2\pi/N)n}$ (2-3b)
Discrete Fourier transform (DFT) of finite-length sequence x(n) of length N into the sequence X(k) of length N	$x(n) = \frac{1}{N}\sum_{k=0}^{N-1} X(k)e^{jk(2\pi/N)n}$, for $0 \le n \le N-1$; $x(n) = 0$, otherwise. (2-4a)	$X(k) = \sum_{n=0}^{N-1} x(n)e^{-jk(2\pi/N)n}$, for $0 \le k \le N-1$; $X(k) = 0$, otherwise. (2-4b)

TABLE 3 Conditions for the Special Case Where There is Exact Correspondence (to within a Scaling Factor) of Fourier Transform of a Continuous-Time Signal and DFT of a Sequence Derived from Sampling [10].

Conditions
(1) The continuous-time signal $x_a(t)$ must be periodic.
(2) The frequency content of $x_a(t)$ must be bandlimited.
(3) The sampling frequency must be greater than twice the largest frequency component of $x_a(t)$.
(4) The sampling length must truncate $x_a(t)$ with a truncation interval exactly equal to one period (or integer multiple of one period) of $x_a(t)$.

TABLE 4 Convolution Representations of Continuous-Time Signals and of Sequences.

Convolution Representation	Definition	Fourier Representation of Convolution
Linear convolution of continuous-time signals $x_{a1}(t)$ and $x_{a2}(t)$	$x_{a3}(t) = \int_{-\infty}^{\infty} x_{a1}(\tau)x_{a2}(t-\tau)d\tau$ (4-1a)	$X_{a3}(j\Omega) = X_{a1}(j\Omega)X_{a2}(j\Omega)$ (4-1b)
Periodic convolution of periodic sequences $\tilde{x}_1(n)$ and $\tilde{x}_2(n)$, each of period N	$\tilde{x}_3(n) = \sum_{m=0}^{N-1} \tilde{x}_1(m)\tilde{x}_2(n-m)$ (4-2a)	$\tilde{X}_3(k) = \tilde{X}_1(k)\tilde{X}_2(k)$ (4-2b)
Circular convolution of finite-length sequences $x_1(n)$ and $x_2(n)$, each of length N. The sequences are represented as periods of periodic sequences $\tilde{x}_1(n)$ and $\tilde{x}_2(n)$, each of period N.	$x_3(n) = \sum_{m=0}^{N-1} \tilde{x}_1(m)\tilde{x}_2(n-m)$, for $0 \le n \le N-1$; $x_3(n) = 0$, otherwise. (4-3a)	$X_3(k) = \tilde{X}_1(k)\tilde{X}_2(k)$, for $0 \le k \le N-1$; $X_3(k) = 0$, otherwise. This is same as: $X_3(k) = X_1(k)X_2(k)$ (4-3b)
Linear convolution via circular convolution of finite-length sequences $x_1(n)$ with length N_1 and $x_2(n)$ with length N_2. The length of each sequence is increased to N_1+N_2-1 by appending sufficient number of zeroes to each sequence. The resulting sequences are represented as periods of periodic sequences $\tilde{x}_1(n)$ and $\tilde{x}_2(n)$, each of period N_1+N_2-1	$x_3(n) = \sum_{m=0}^{N_1+N_2-2} \tilde{x}_1(m)\tilde{x}_2(n-m)$ for $0 \le n \le N_1+N_2-2$; $x_3(n) = 0$, otherwise. (4-4a)	$X_3(k) = X_1(k)X_2(k)$, for $0 \le k \le N_1+N_2-2$; $X_3(k) = 0$, otherwise. (4-4b)

TABLE 5 Significance of Sampling Parameters for Deriving a Sequence from Sampling a Continuous-Time Signal.

Sampling Parameter	Significance	Relationship
Sampling frequency 1/T, where T is sampling period in sec and 1/T is frequency in Hz.	To avoid distortion due to aliasing, the sampling frequency must be larger than twice the highest frequency component contained in the continuous-time signal.	$\frac{\Omega_o}{2} < \frac{\pi}{T}$ (5-1) where $\Omega_o/2$ is the maximum radian frequency of the continuous-time signal.
Sampling length* NT, where N is length of the sequence derived from sampling and T is sampling period in sec.	To improve DFT frequency domain resolution, the sampling length must be increased.	Frequency resolution (Hz) $= 1/(NT)$ (5-2)
	To avoid distortion due to "leakage" [23,25] resulting from truncating the signal, the sampling length must be sufficient to totally contain the signal.**	$NT \geq$ Time duration of signal (5-3)
	To utilize the best efficiency of FFT computation, N should be an integer power of 2.	$N = 2^{\nu}$ (5-4) where ν is an integer.

* If the sequence is to encounter a linear convolution evaluation using circular convolution via a FFT algorithm, appended zeroes may be required to extend the length of the sequence.

** If the signal is periodic, the sampling length should be equal to the period or an integer multiple of the period. If truncation can not be avoided, the truncation effects should be minimized by smoothing the signal by proper time windowing [7-10].

TABLE 6 Program Listing for Microcomputer-Based N-Point FFT and IFFT Computations in BASIC when N is an Integer Multiple of 2.

```
30000 rem     Subroutine to calculate Fast Fourier Transform (FFT)
30010 rem           or Inverse Fast Fourier Transform (IFFT)
30020 rem
30030 rem     Data are in fr(real) and fi(imaginary) arrays
30040 rem     Calculation is in place,output replaces input
30050 rem     The following parameters must be defined :
30060 rem         nfft%    :  The number of points (must be power of 2)
30070 rem         itr%     :  1 for FFT, -1 for IFFT
30080 rem -----------------------------------------------------------------
30090 rem     Check if nfft% is integer power of 2
30100 xnfft=nfft%
30110 for i%=1 to 20
30120 xnfft=.5*xnfft : if xnfft=1 then 30170
30130 if xnfft>1 then 30160
30140 print " ERROR in subroutine FFT ( nfft%  wrong !!! ) " : print
30150 stop
30160 next i%
30170 rem     Check itr%
30190 if itr%=1 or itr%=-1 then 30220
30200 print " ERROR in subroutine FFT ( itr% wrong !!! ) " : print
30210 stop
30220 rem     Calculate FFT
30230 mr%=0 : nn%=nfft%-1
30240 for m%=1 to nn%
30250 nl%=nfft%
30260 nl%=nl%\2 : if mr%+nl%>nn% then 30260
30270 mr%=(mr% mod nl%)+nl% : if mr%<=m% then 30300
30280 tr=fr(m%+1) : fr(m%+1)=fr(mr%+1) : fr(mr%+1)=tr
30290 ti=fi(m%+1) : fi(m%+1)=fi(mr%+1) : fi(mr%+1)=ti
30300 next m%
30310 nl%=1
30320 if nl%>=nfft% then 30440
30330 istep%=nl%+nl% : el=nl%
30340 for m%=1 to nl%
30350 arg=3.141593*(itr%*(1-m%))/el : wr=cos(arg) : wi=sin(arg)
30360 for i%=m% to nfft% step istep%
30370 j%=i%+nl%
30380 tr=wr*fr(j%)-wi*fi(j%) : ti=wr*fi(j%)+wi*fr(j%)
30390 fr(j%)=fr(i%)-tr : fi(j%)=fi(i%)-ti
30400 fr(i%)=fr(i%)+tr : fi(i%)=fi(i%)+ti
30410 next i%
30420 next m%
30430 nl%=istep% : goto 30320
30440 if itr%=1 then return
30450 for i%=1 to nfft%
30460 fr(i%)=fr(i%)/nfft% : fi(i%)=fi(i%)/nfft%
30470 next i%
30480 return
```

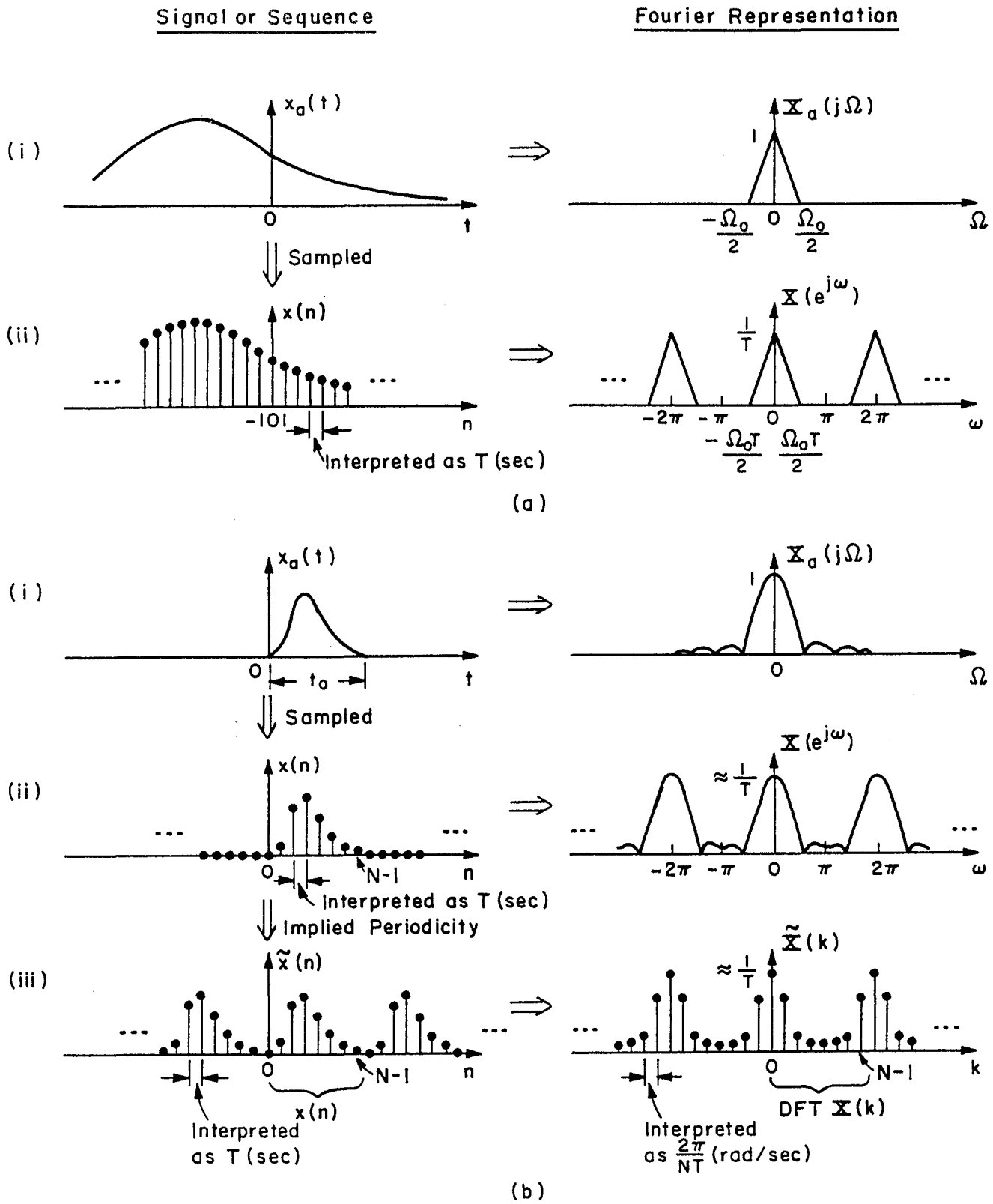

Fig. 1 Fourier representations of (a) continuous-time signal and sequence derived from sampling, and of (b) finite-duration continuous-time signal, sequence derived from sampling and the sequence with implied periodicity.

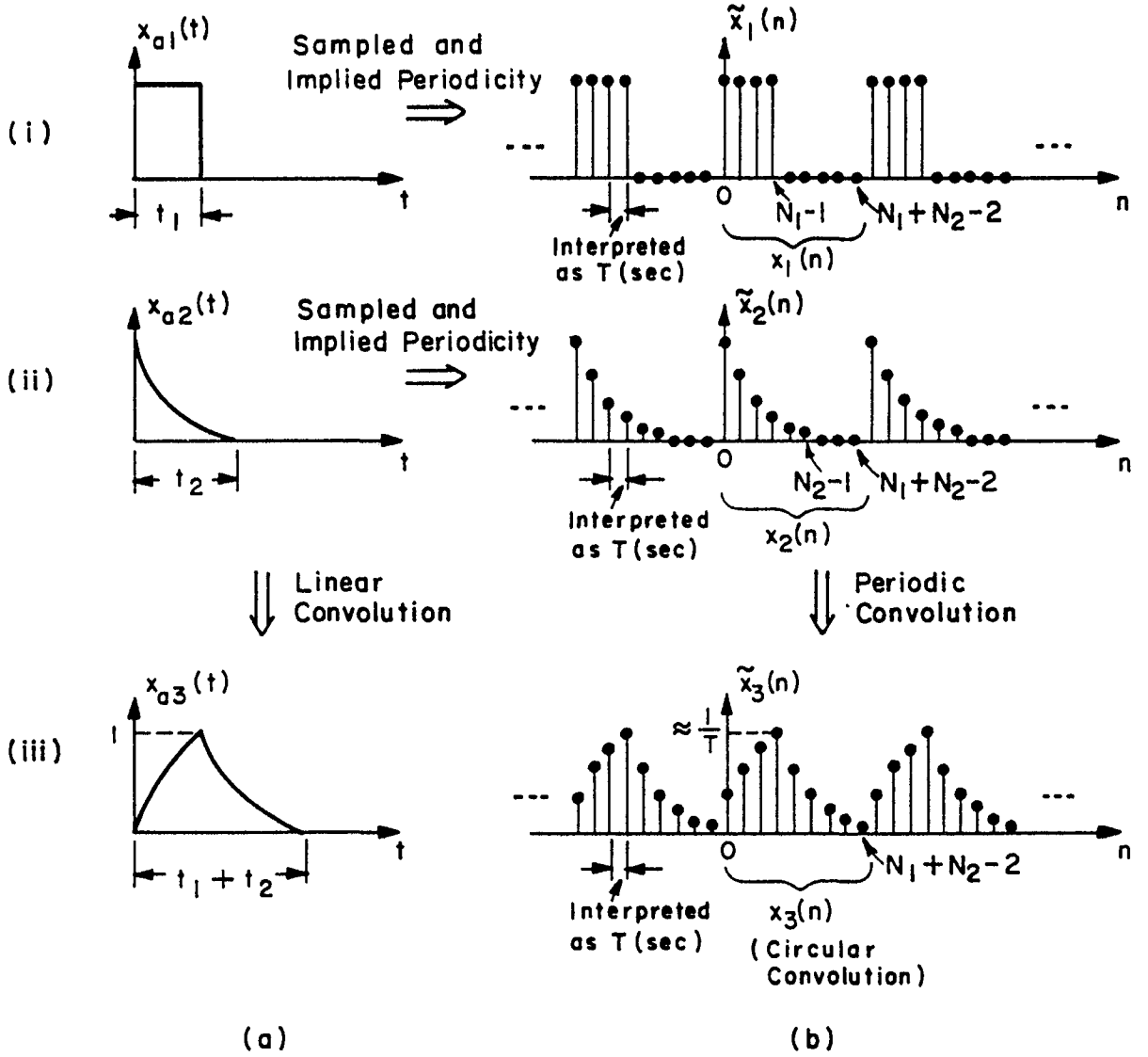

Fig. 2 (a) Linear convolution of continuous-time signals and (b) circular convolution of sequences derived from sampling the signals.

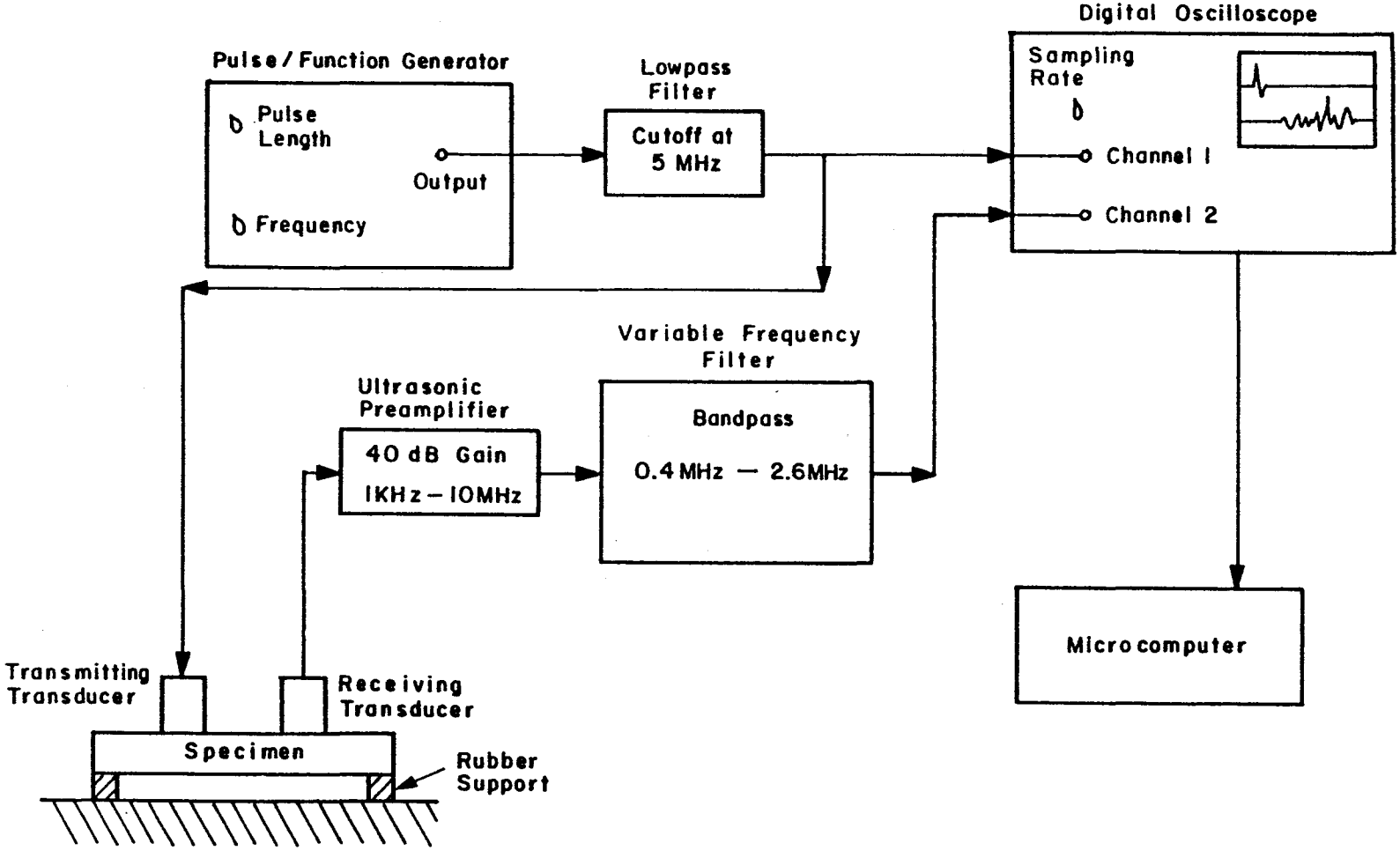

Fig. 3 Schematic of experimental components with specimen showing the "stress wave factor" test configuration. (All tests in this study were conducted with transducers coupled face to face without a test specimen.)

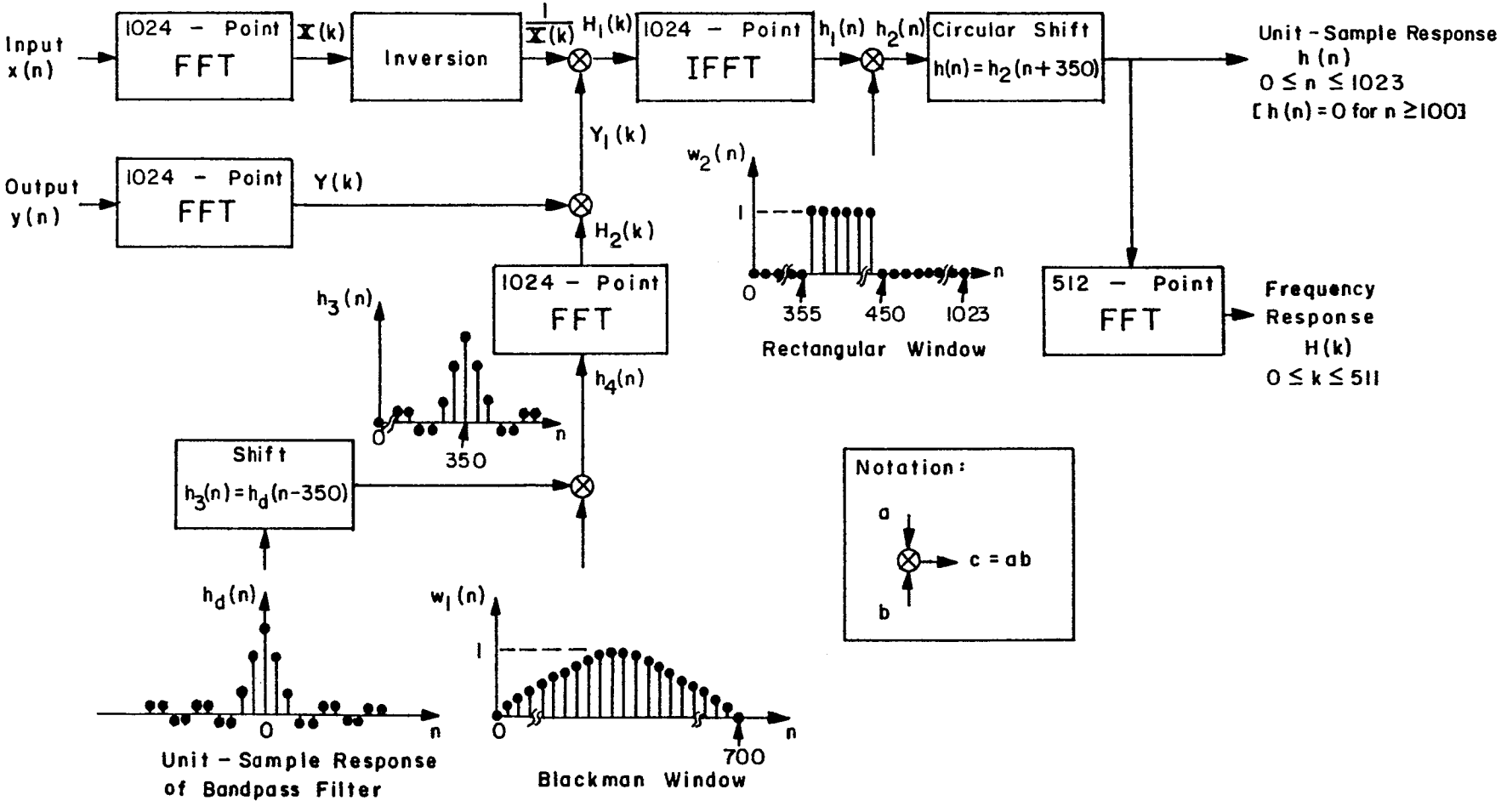

Fig. 4 Schematic of digital signal processing procedures applied to experimental input and output sequences to evaluate unit-sample response and frequency response of experimental system.

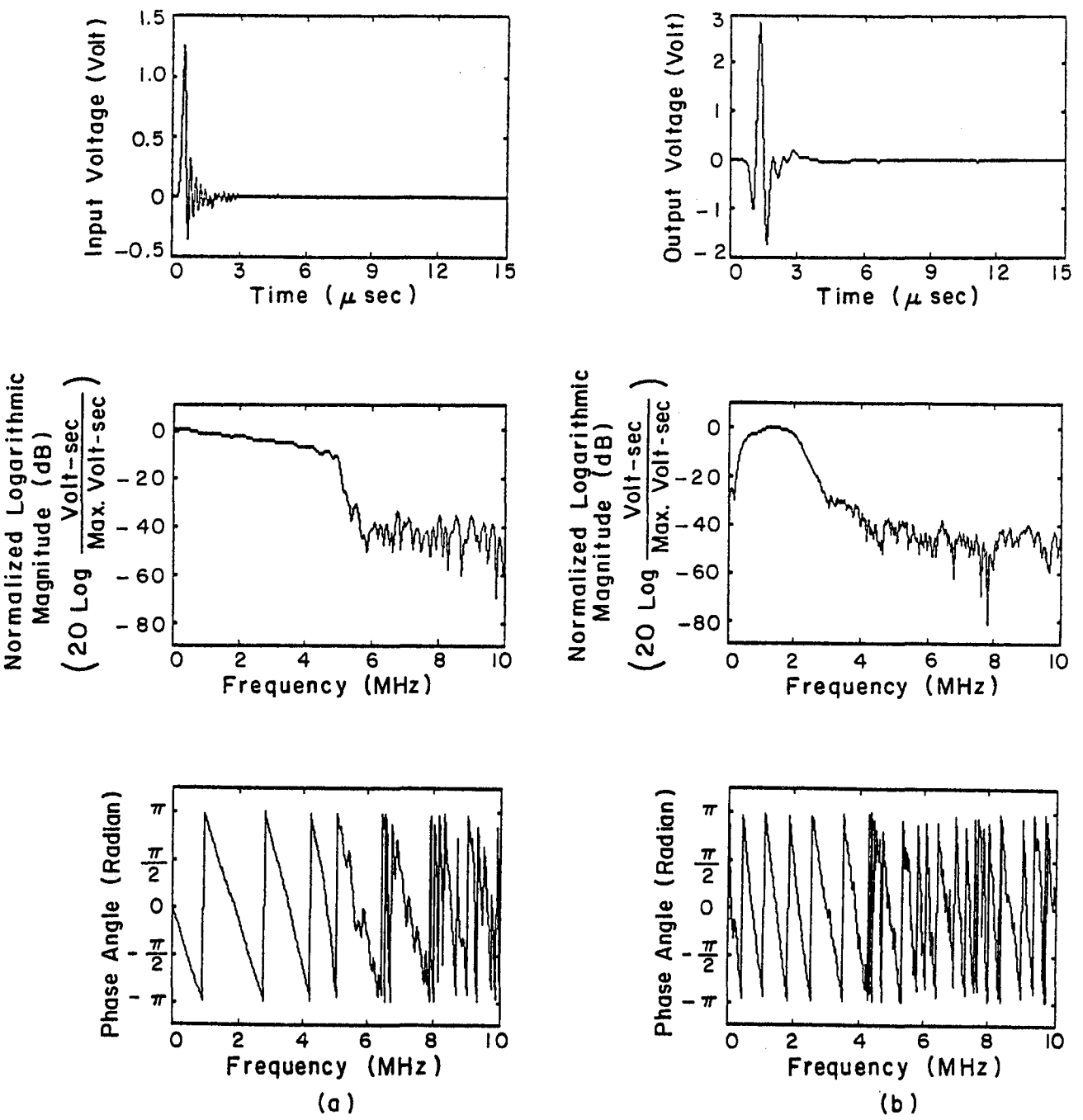

Fig. 5 Time history, magnitude and phase of (a) input signal and (b) output signal.

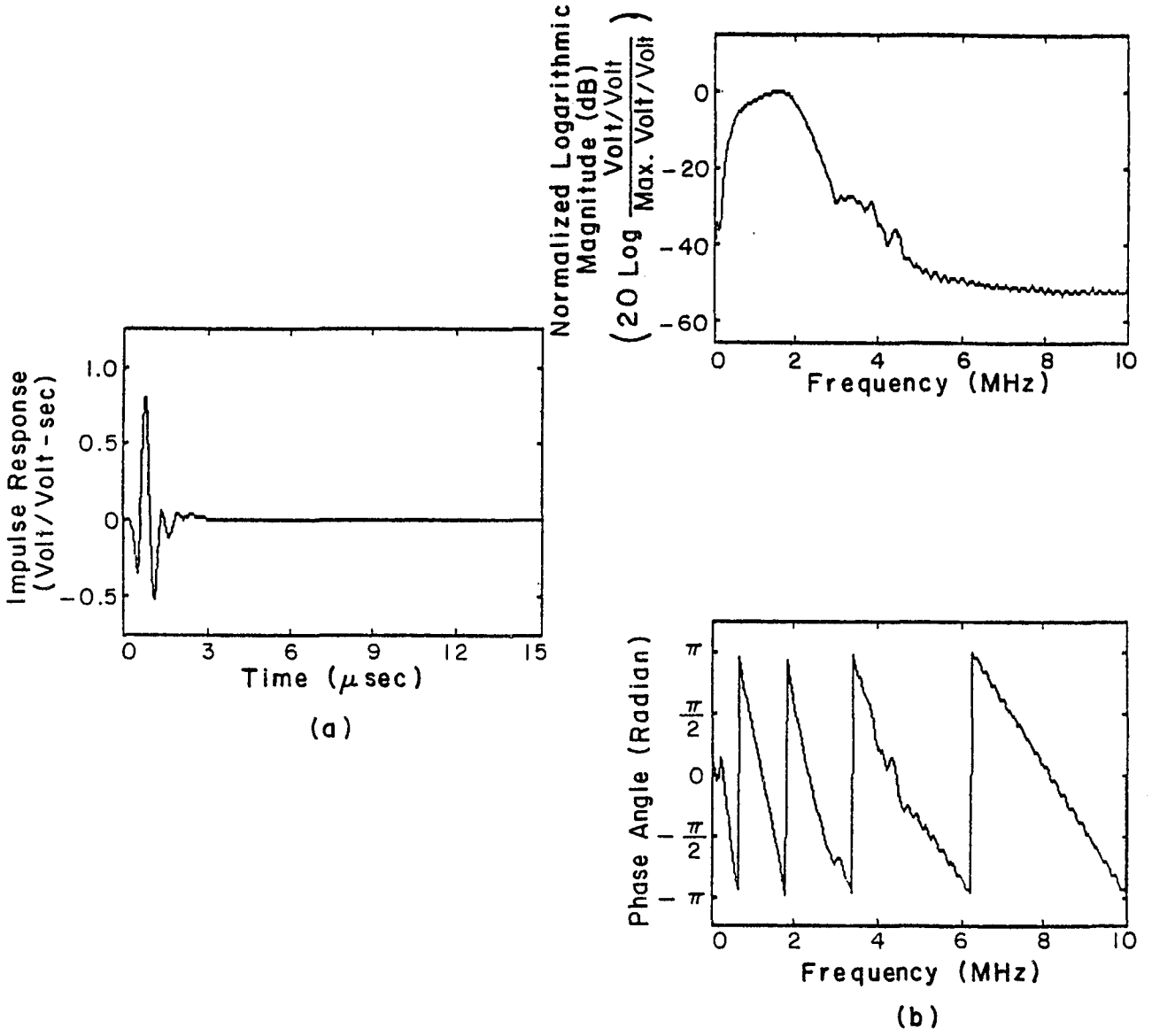

Fig. 6 Experimentally determined (a) impulse response and (b) frequency response of test system.

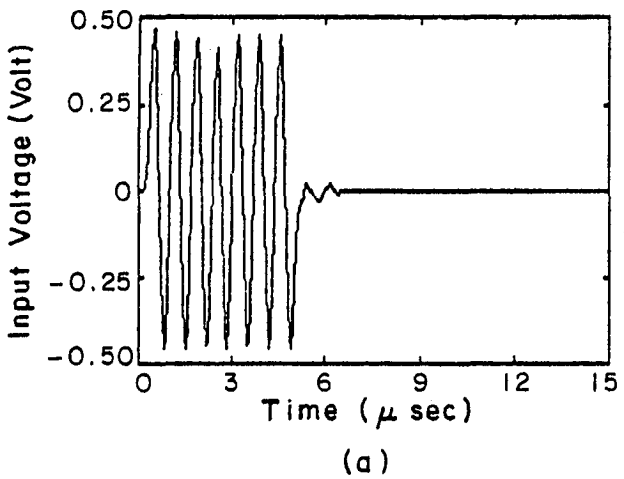

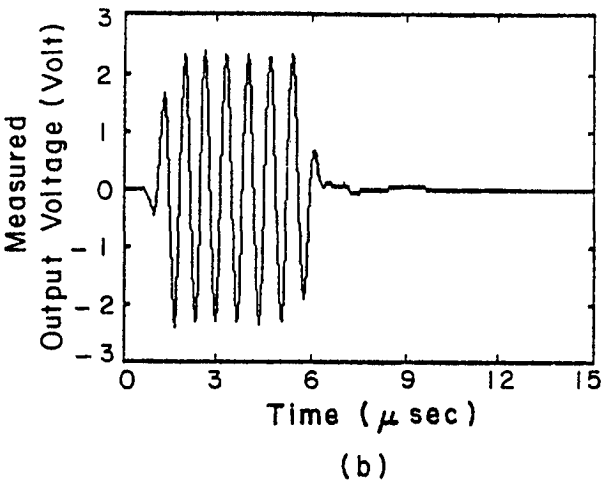

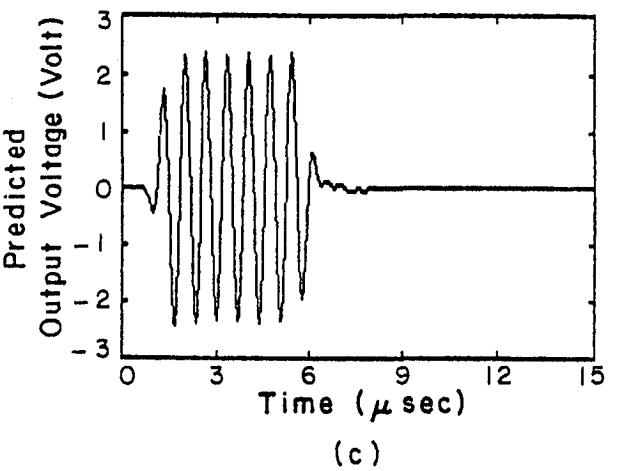

Fig. 7 Measured and predicted system responses: (a) 1.5 MHz center frequency tone burst input and corresponding (b) experimental output and (c) predicted output.

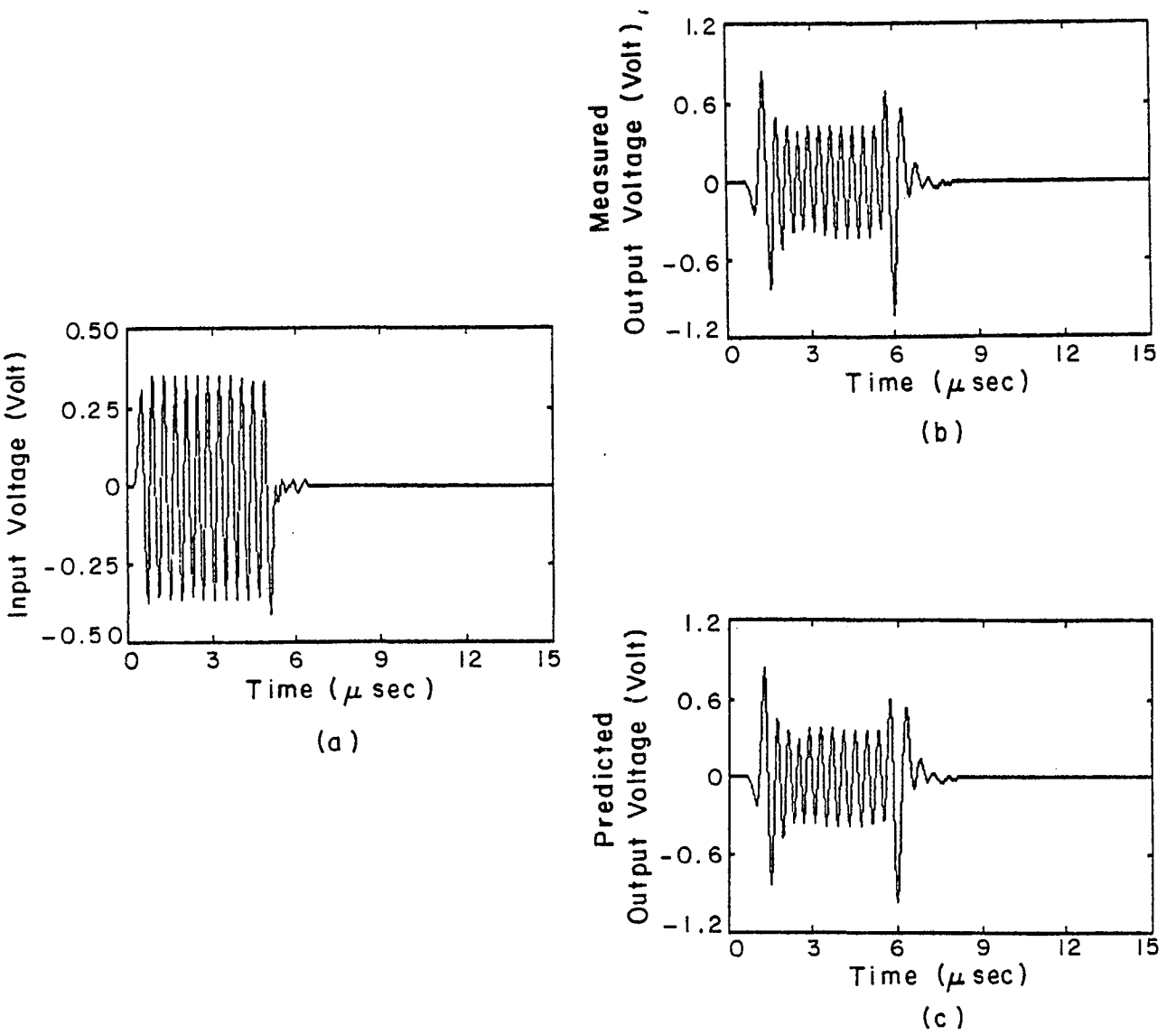

Fig. 8 Measured and predicted system responses: (a) 2.5 MHz center frequency tone burst input and corresponding (b) experimental output and (c) predicted output.

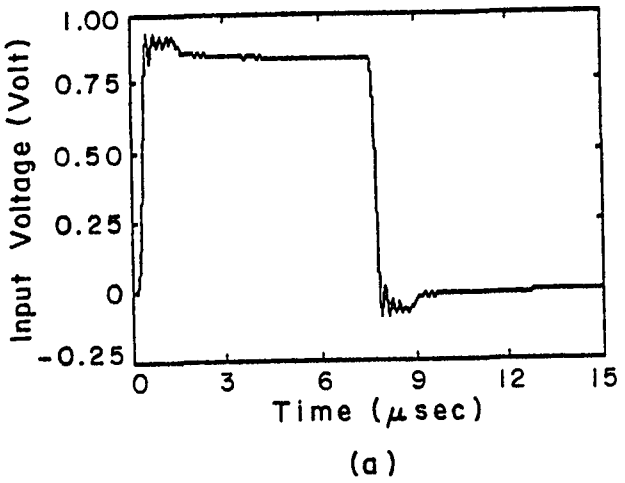

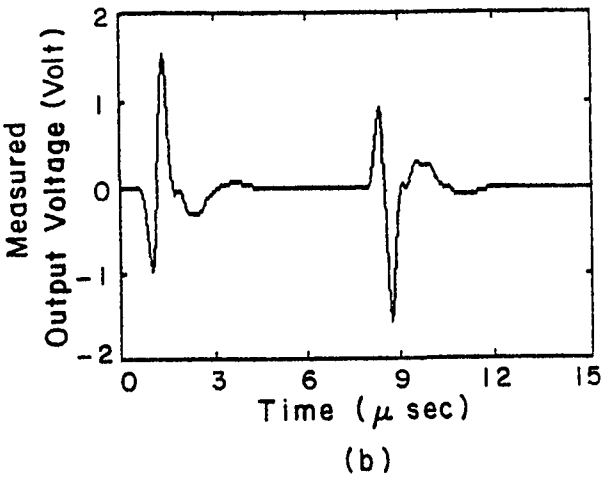

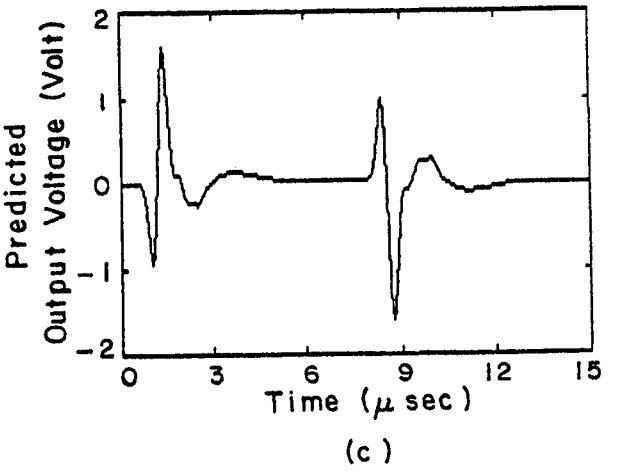

Fig. 9 Measured and predicted system responses: (a) 7.65 μsec duration rectangular pulse input and corresponding (b) experimental output and (c) predicted output.

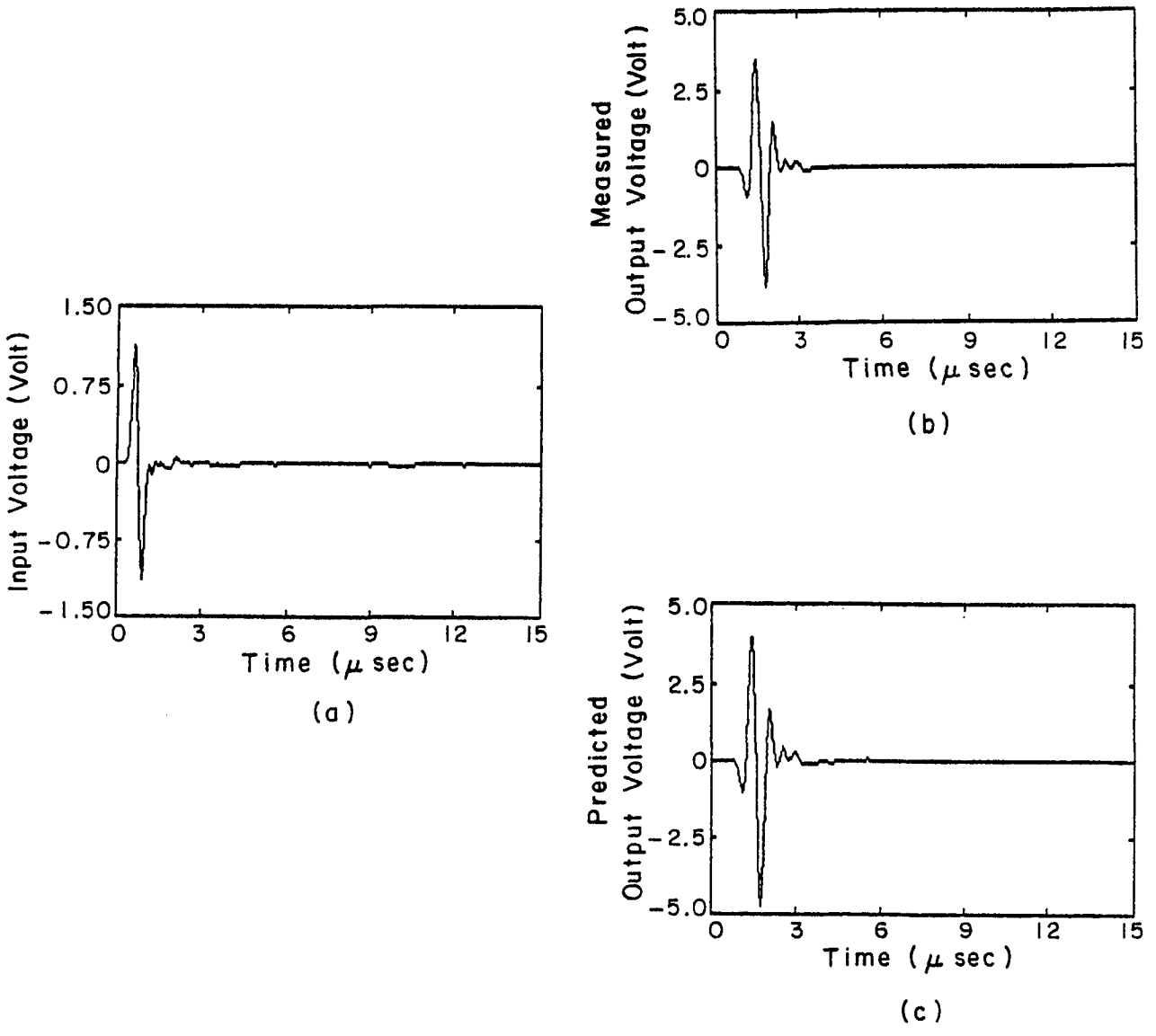

Fig. 10 Measured and predicted system responses: (a) One cycle of 1.75 MHz frequency input at 2.3 Volts peak-to-peak and corresponding (b) experimental output and (c) predicted output.